

# Temperature-Induced Formation of a Non-Native Intermediate State of the All $\beta$ -Sheet Protein CD2

Jenny J. Yang,<sup>\*,1</sup> Haidong Yang,<sup>2</sup> Yiming Ye,<sup>1</sup>  
Harry Hopkins, Jr.,<sup>1</sup> and Gary Hastings<sup>3</sup>

<sup>1</sup>Department of Chemistry, Center of Drug Design, <sup>2</sup>Department of Biology,  
and <sup>3</sup>Department of Physics and Astronomy, Georgia State University, Atlanta, GA, 30303

## Abstract

Domain 1 of the cell adhesion protein CD2 (CD2-1) has an all  $\beta$ -structure typical of proteins belonging to the immunoglobulin superfamily. It has a remarkable ability to fold as a native monomer or a metastable intertwined dimer. To understand the origin of structural rearrangements of CD2-1, we have studied equilibrium unfolding of the protein using various biophysical spectroscopic techniques. At temperatures above approx 68°C, a partially folded state of CD2-1 (H state) with a distinct secondary structure, involving largely exposed aromatic and hydrophobic residues and a substantially perturbed tertiary structure, is observed. In contrast, an unfolded state (D state) of CD2-1 with random-coil-like secondary and tertiary structures is observed in 6 M GuHCl. This partially folded high-temperature state has increased negative molar ellipticity at 222 nm in far-ultraviolet CD spectra, implying formation of a non-native helical conformation. The existence of this non-native high-temperature intermediate is consistent with relatively high intrinsic helical propensities in the primary sequence of CD2-1. This conformational flexibility may be important in the observed domain swapping of CD2-1.

**Index Entries:** Folding of  $\beta$ -sheet proteins; thermal denaturation; domain swapping; non-native intermediate; quantitative protein secondary structural analysis.

The mechanism of protein folding is currently an important question in chemistry and biology. The study of the mechanism by which proteins fold into precise three-dimensional structures provides a deeper understanding of the protein-folding problem. Folding of an extended polypeptide chain on the second to

minute time scale suggests that folding follows pathways defined by multidimensional energy landscapes (1–3). A limited number of intermediate folding states and multiple folding pathways have been outlined for a few proteins (4–7). One incisive approach defining a sequence of protein-folding events is to characterize physical properties of structurally and energetically stable intermediate states at equilibrium conditions (8,9). Equilibrium unfolding of a protein by chemical denaturants, pH, or

\* Author whom all correspondence and reprint requests should be addressed. E-mail: chejy@panther.gsu.edu

temperature allows us to identify determinants for stabilization of folding intermediates and to answer how the hierarchy of structural levels governs both the conformational stability and the folding/unfolding pathways of proteins. One key folding intermediate is called the molten globule, and this has been found in the folding pathways of many proteins, such as myoglobin and  $\alpha$ -lactalbumin (4,10–14). The molten globule has a significant native-like secondary structure but a largely flexible tertiary structure with exposed hydrophobic surfaces (4,8,15). This equilibrium molten-globule state has been shown to be a relevant kinetic intermediate both in vivo and in vitro (16–18). Proteins with fewer than 100 amino acid residues fold without a detectable intermediate state (19,20). In contrast, proteins with over 100 amino acids in length do fold via stable intermediates (21–23).

Several advances in the folding of  $\beta$ -sheet proteins have been achieved by using peptide models, mutagenesis, and design approaches (19,24). Unlike the folding of an  $\alpha$ -helix, the folding of a  $\beta$ -sheet requires the formation of peptide hydrogen bonds between two or more polypeptide segments that may be far apart in the linear sequence. As pointed out in several reviews, in-depth folding studies on all  $\beta$ -sheet proteins provide more direct evidence for understanding how the rapid formation of the specific H-bonding networks by remote residues is initiated or how local and long-range interactions contribute to the final formation of  $\beta$ -sheet structures (24,25). Small, all  $\beta$ -sheet proteins with high solubility offer good systems for the study of  $\beta$ -sheet folding (26–29).

The domain 1 of rat CD2 (CD2-1) is an all  $\beta$ -sheet protein and is an ideal model system for understanding the key determinants for the folding of  $\beta$ -sheet proteins (30–33). CD2-1 is a cell surface receptor on natural killer cells and plays an important role in mediating both cell adhesion in T-lymphocytes and signal transduction (34–36). Only domain 1 of CD2 is involved in adhesion. CD2-1 is small (99 amino acids), highly soluble, and lacks disulfide bonds. Structural studies have shown that

CD2-1 has a common Greek key architecture shared by the immunoglobulin family (Fig. 1) (34–36). As shown in Fig. 1, CD2-1 contains two Trp residues. Trp-32 is completely buried in the hydrophobic core of the protein. In contrast, Trp-7 on strand A is largely exposed to solvent. The two Trp residues can serve as internal probes to trace the change of the tertiary structure of CD2-1 and to gauge the opening of the two layers of sheets by fluorescence and near-ultraviolet (UV) circular dichroism (CD) methods.

CD2-1 has the remarkable ability to fold either as a native monomer or as an intertwined, metastable dimer (37). About 15% of the recombinant protein was observed as a dimer when expressed as a glutathione-S-transferase (GST) fusion protein. This dimeric form of CD2-1 can be refolded back into a monomer by GuHCl in the absence of the GST fusion partner (37). Crystallographic studies reveal that this dimer has an unusual fold with two interexchanged polypeptide chains entangled head to tail. More dramatically, the intertwined dimer can be stabilized by deleting two residues at the C'' hinge region of CD2-1 and a tetramer can be further assembled (38). Based on these observations, Murray et al. proposed the existence of a loosely folded (molten globule) intermediate that has the features necessary to be a common precursor to both monomer and dimer structures (37–39). We have shown that domain 1 of CD2 can be converted to be significantly helical in the presence of TFE (40).

Here, we report our unfolding studies of CD2-1 with the aim of identifying the determinants for the conformational properties of all  $\beta$ -sheet proteins and understanding the origin of the structural rearrangement of CD2-1 by exploring equilibrium intermediates. Various biophysical techniques that are sensitive to the change of different levels of protein structures have been employed. A partially folded state with some molten-globular characteristics has been observed at high temperatures (denoted as the H state). We have observed that part of the residues in the

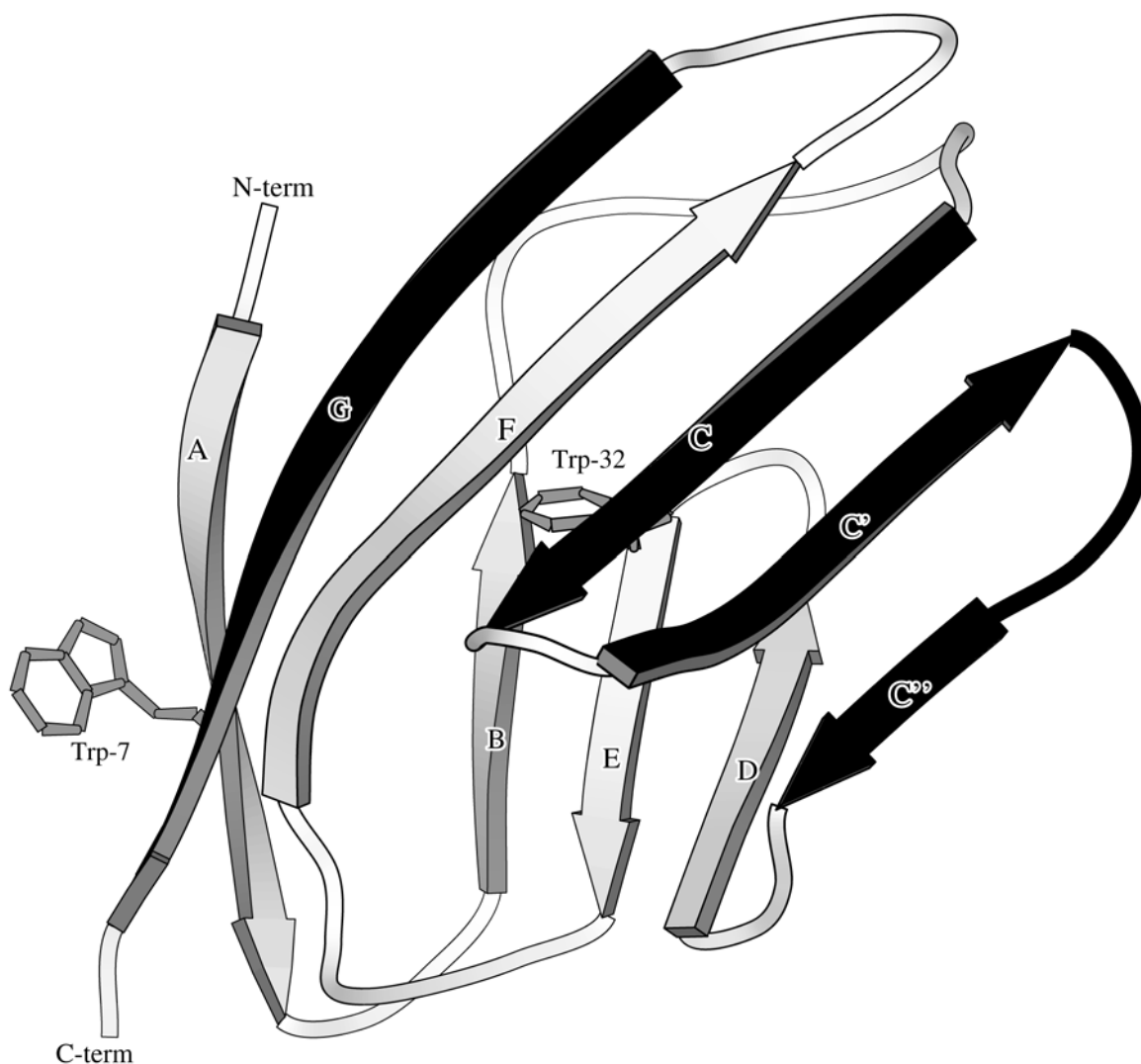


Fig. 1. Schematic representation of the three-dimensional structure of domain 1 of rat CD2 (35). The side chains of tryptophan residues 7 and 32 are shown in wireframe representation. Secondary structure prediction based on the amino acid sequence of domain 1 of rat CD2 was carried out using three algorithms (PHD, GOR, and SOMPA) (40). Residues with strong  $\beta$ -sheet propensities are labeled in gray. Residues with strong  $\alpha$ -helix propensities are labeled in black.

native  $\beta$ -sheet conformation was converted to a helical conformation. The origins of this conformational change were investigated by analyzing the intrinsic secondary structure propensity of CD2-1. The relevance of this intermediate to the conformational flexibility of CD2-1 and the domain-swapping metastable structure is also discussed.

## RESULTS AND DISCUSSION

One way to perturb the equilibrium between different conformational species in proteins is to change the temperature (22). To explore if an equilibrium intermediate of CD2-1 can be induced by thermal denaturation, we have used CD, Fourier-transform infrared (FTIR),

and fluorescence spectroscopy in conjunction with differential scanning calorimetry (DSC). These multiple probes can be used to gain insight into the changes of secondary and tertiary structures of the protein and explore the cooperativity of folding. Concentration ranges from 2 to 200  $\mu\text{M}$  were selected for thermal denaturation studies. At these concentrations, aggregation was not observed up to 90°C.

### ***Unpacking of Tertiary Structure of CD2-1 Induced by Temperature***

Near-UV CD signals of proteins mainly originate from the asymmetric environment around aromatic residues (41). Rat CD2-1 contains two tryptophan (Trp-7 and Trp-32), two tyrosine (Tyr-76, and Tyr-81), four phenylalanine (Phe-21, Phe-42, Phe-49, and Phe-55), and one histidine residues (His-12). To investigate the effects of temperature on the tertiary structure of CD2-1, the near-UV CD spectra of 45  $\mu\text{M}$  CD2-1 in phosphate-buffered saline (PBS) at pH 7.3, at different temperatures were recorded. Samples were allowed to equilibrate at each temperature for 20 min (Fig. 2A). Native CD2-1 at 25°C has a complex near-UV CD spectrum with negative maxima at 265, 281, and 289 nm. This complexity reflects the high proportion of aromatic residues (10) in the protein. Elevating the temperature decreases the intensity of the near-UV CD signals at 281 nm and 289 nm (Fig. 2A). At temperatures higher than 70°C, almost all of the near-UV signals are diminished, suggesting that the asymmetric environment of the aromatic residues of CD2-1 are severely perturbed by thermal denaturation.

Fluorescence spectroscopy is very sensitive to the change of the environment of aromatic amino acid residues. Because Trp-32 is located at the center of the hydrophobic core of CD2 and is fully buried (Fig. 1), intrinsic Trp fluorescence was used as a tertiary structural probe for the (un) folding of CD2-1. Excited at 280 nm, the emission spectrum of native CD2-1 has two emission maxima at 318 and 328 nm at 25°C (Fig. 2B). These two emission maxima may reflect the

large difference in the environment of the two Trp residues in the native protein. Increasing the temperature substantially decreases the Trp fluorescence intensity at 328 nm (about 70%). In addition, the two emission maxima at 318 nm and 328 nm at 25°C are evolved and shifted to a single maximum at 348 nm at 80°C. To dissect the contribution of the conformational change of CD2-1 to the Trp fluorescence by denaturation, 4  $\mu\text{M}$  amino acid Trp was used as a control for 2  $\mu\text{M}$  of the protein containing two Trp residues. The effects of temperature on the fluorescence spectra of free amino acid Trp were examined under identical experimental conditions. Although increasing the temperature from 25°C to 80°C results in about a 52% decrease of the Trp fluorescence intensity of the free amino acid, the emission maximum of free Trp remains at 355 nm. This emission maximum is close to that of CD2-1 at 80°C. Results from near-UV CD and Trp fluorescence temperature studies suggest that the tertiary structure of CD2-1 (H state) is severely perturbed and the aromatic amino acid residues are largely exposed to the solvent at high temperatures.

To investigate unpacking of the tertiary structure of CD2-1 at high temperature resulting in the exposure of hydrophobic clusters, we have measured the fluorescence of the hydrophobic probe 1-anilinonaphthalene-8-sulfonate (ANS) in the presence and absence of protein at different temperatures. As shown in Fig. 3, a blue-shift of 10 nm in the  $\lambda_{\text{max}}$  of ANS fluorescence and a twofold increase in its intensity occurs upon the addition of CD2-1 at 80°C. By contrast, less than a 5% change of ANS fluorescence was observed upon the addition of CD2-1 at 25°C or in the presence of 6 M GuHCl. These results suggest that the thermal-induced H state of CD2-1 possesses a hydrophobic surface that binds ANS and resembles the molten-globule state observed in many proteins (4,10–14).

### ***Non-native Secondary Structure of CD2-1 Induced by Temperature***

Far-UV CD is very sensitive to the polypeptide backbone conformations of proteins. As

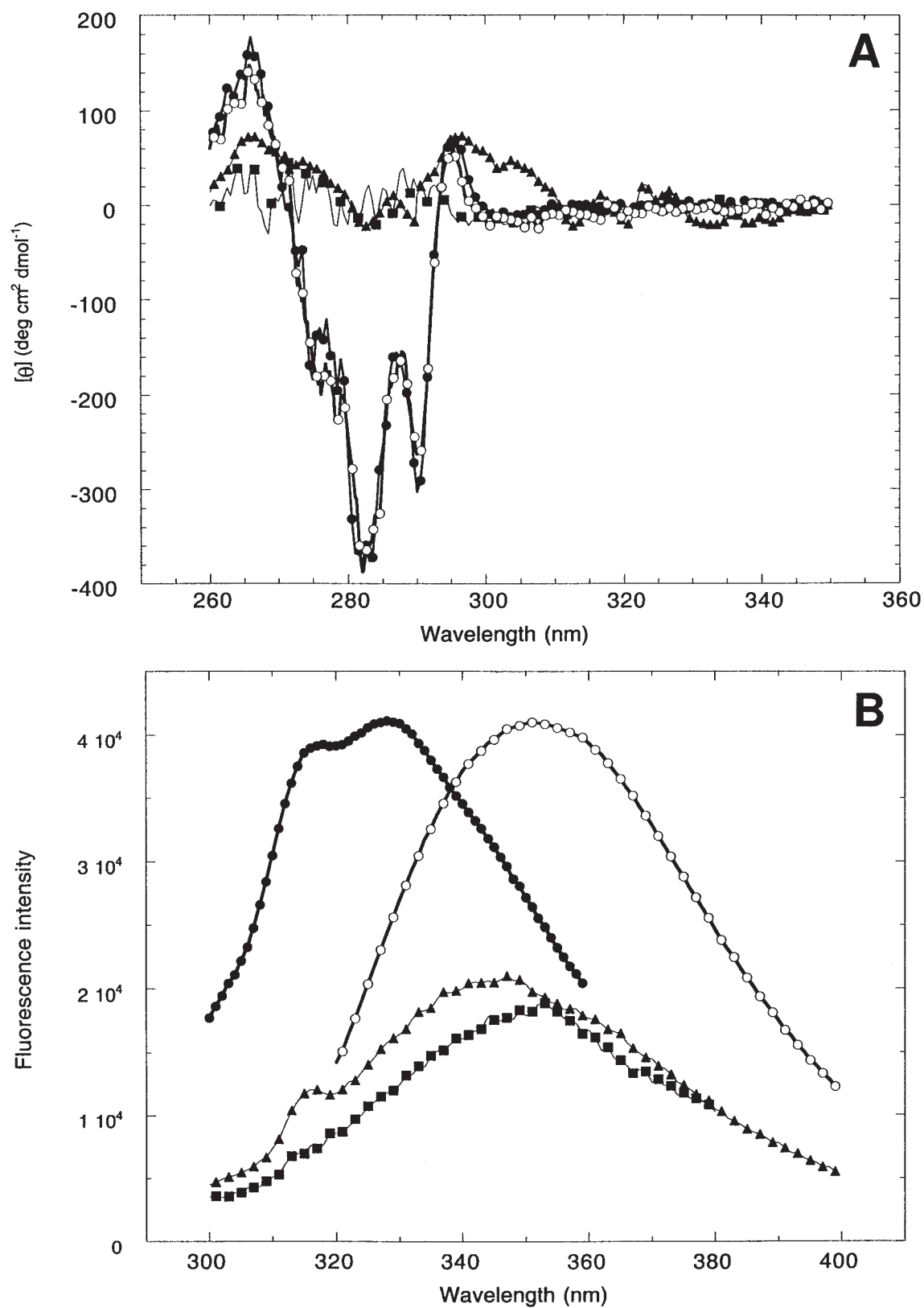


Fig. 2. (A) The near-UV CD spectra (45  $\mu$ M) of CD2-1 in PBS buffer (pH 7.3) at 25°C (●), in 6.0 M GuHCl at 25°C (■) in PBS buffer (pH 7.3) at 80°C (▲), and in PBS buffer (pH 7.3) at 25°C after staying at 80°C for 45 min (○). (B) The emission (excited at 280 nm) spectra of 2  $\mu$ M CD2-1 at 25°C (●), and 80°C (▲) in PBS buffer, and in 6.0 M GuHCl at 25°C (■). The emission spectrum (excited at 280 nm) of 4  $\mu$ M free amino acid Trp (○) at 25°C in PBS buffer (pH 7.3).

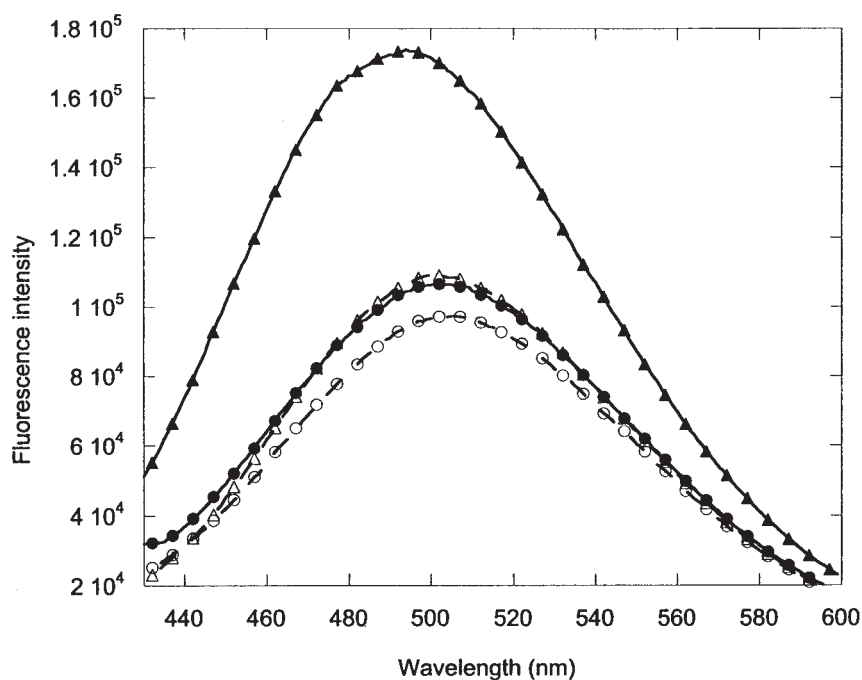


Fig. 3. The fluorescence emission spectra of 0.1 mM ANS in the absence (dashed line) (○) and presence of 20  $\mu$ M CD2-1 (solid line) at 25°C. (●), ANS in PBS buffer (pH 7.3) in the absence (△) and presence of 20  $\mu$ M CD2-1 (▲) at 80°C.

shown in Fig. 4, the far-UV CD spectrum of native CD2-1 (45  $\mu$ M) at 25°C has a negative maximum at 215 nm, which resembles closely that of domain 1 and domain 2 of human CD2 and CD4 (42,43) and pseudoazurin (44). All of these proteins share a high similarity in three-dimensional structures and topology with a Greek key  $\beta$ -sandwich (34,35,45,46). The relatively small intensity (about  $-3000$  deg  $\text{cm}^2/\text{dmol}$ ) at the negative maximum for these proteins is likely a result of the twisting of strands in proteins and the influence from aromatic contribution (41,43,47,48).

To investigate the effect of temperature on the secondary structure of CD2-1, the far-UV CD spectra of 45  $\mu$ M CD2-1 in PBS buffer at different temperatures were recorded under the same conditions as for the near-UV CD studies (Fig. 4). Surprisingly, increasing the temperature increases the molar ellipticity at 222 nm. Concurrently, the width of the CD band becomes broader and its negative maximum at

215 nm evolves into two negative maxima at 210 and 220 nm at 80°C. Increasing the temperature to 90°C does not induce any additional change in the far-UV CD spectrum of CD2-1. From 25°C to 80°C, the ellipticity at 222 nm of CD2-1 is enhanced about 1.5-fold, which is in strong contrast to the diminished CD signal observed in 6 M GuHCl. The distinct far-UV CD spectrum with the temperature-induced enhancement of negative molar ellipticity at 222 nm is *not* commonly observed for many proteins. Some proteins only exhibit a small residual CD signal at 222 nm when exposed to thermal denaturation (18,49–53).

There are several possible explanations for the H-state conformation and the corresponding negative increase of the far-UV CD signal at 222 nm at high temperature. First, the negative increase in ellipticity may be the result of protein oligomerization. To investigate this possibility, we have measured the far-UV CD spectra, and one-dimensional nuclear magnetic resonance (NMR)

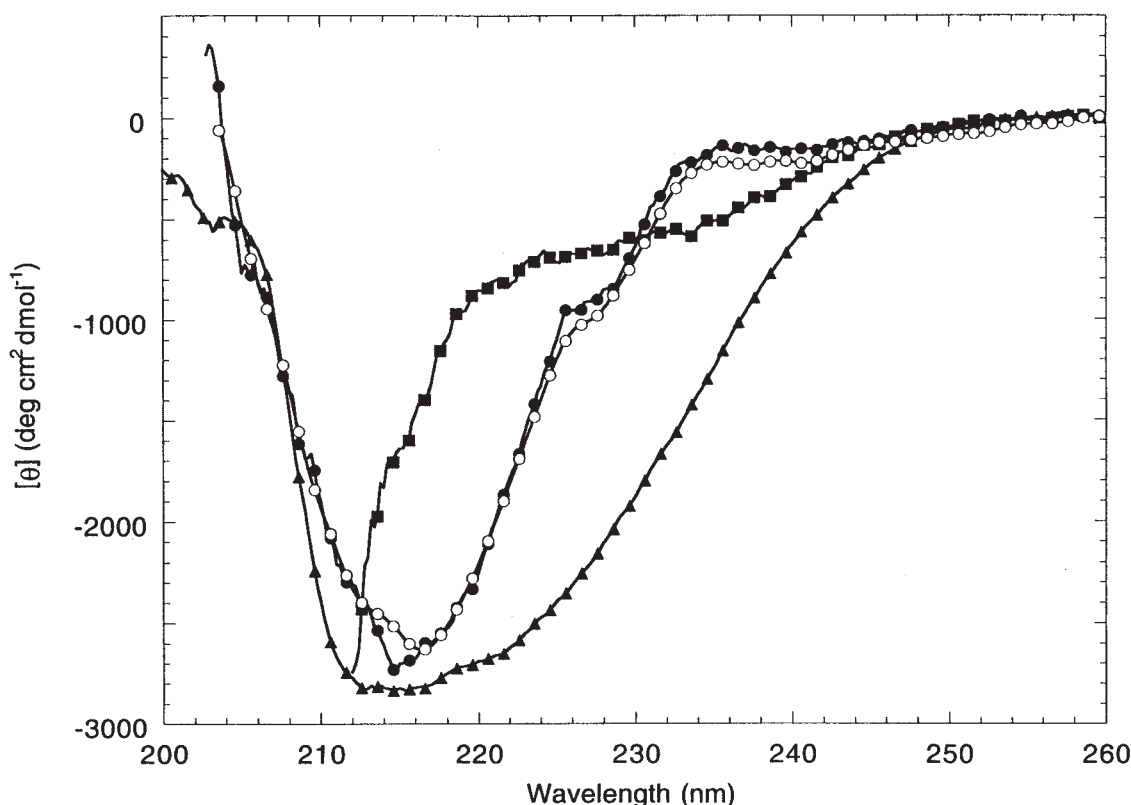


Fig. 4. The far-UV CD spectra of 45  $\mu\text{M}$  CD2-1 at different conditions: in PBS buffer (pH 7.3) at 25°C (●), in 6.0 M GuHCl at 25°C (■), in PBS buffer (pH 7.3) at 80°C (▲), and in PBS buffer (pH 7.3) at 25°C after staying at 80°C for 45 min (○).

spectra, of CD2 as a function of protein concentration at high temperature (data not shown). There is no concentration dependence of the temperature-induced molar ellipticity at 222 nm from 1.0 to 80  $\mu\text{M}$ . In addition, the NMR linewidth of CD2 is not changed from 50 to 200  $\mu\text{M}$  at 90°C. Taken together, these results suggest that the induced molar ellipticity is less likely to be a result of oligomerization of CD2. The second possibility is that the temperature-induced ellipticity may be due to an increased contribution from aromatic amino acid residues to the far-UV CD signal relating to changes in the tertiary structure of CD2-1. Near-UV CD signal is a result of aromatic residues in an asymmetric environment of a tightly packed protein (43,48,54–56). As suggested from the near-UV CD and Trp fluorescence studies (Fig. 2A,B), the

aromatic residues in the H state are largely exposed to the solvent, and the tight packing of the protein core is severely disturbed (Fig. 2A,B). Hence, the aromatic amino acid contribution for the H state is expected to be dramatically reduced compared to that of the native state of the protein (53). The third and most likely possibility is that the high-temperature-induced ellipticity at 222 nm is the result of the formation of non-native helical conformations. It is well known that an  $\alpha$ -helical conformation has a strong far-UV CD signal at 222 nm, and proteins with 100% helical conformations give molar ellipticity of 33,000  $\text{deg cm}^2/\text{dmol}$  at 222 nm (41,43,47,48,54–59). To further investigate the thermal-induced secondary structure change of the non-native H state of CD2-1, we have used FTIR spectroscopy.

Fourier-transform infrared spectroscopy is a useful tool for the investigation of small secondary structural changes of proteins in aqueous solution (60–66). The so-called amide vibrations are associated with the peptide groups. The amide I absorption band is principally the result of an in-plane C=O stretching vibration. This gives rise to infrared bands between 1600 and 1700  $\text{cm}^{-1}$ . A protein containing several types of secondary structure gives rise to several overlapping amide I absorption bands. The observed amide I band is therefore relatively broad. Sensitive FTIR measurements of proteins, in combination with modern deconvolution and curve-fitting algorithms, have been used successfully to probe the underlying component bands that contribute to the broad amide I transition. From studies of numerous (more than 100) proteins, it was found that distinct elements of secondary structure give rise to specific infrared (IR) absorption bands, over only narrow ranges of frequency (60,67). Quantitative secondary structural information can be derived from the relative strengths of specific absorption bands (63). From studies of 19 proteins, Byler and Susi (67) suggested that bands at  $1653 \pm 4 \text{ cm}^{-1}$  are the result of the  $\alpha$ -helix, whereas bands at  $1624 \pm 4 \text{ cm}^{-1}$ ,  $1631 \pm 3 \text{ cm}^{-1}$ ,  $1637 \pm 3 \text{ cm}^{-1}$ , and  $1675 \pm 5 \text{ cm}^{-1}$  are the result of different  $\beta$ -sheet structures (see also ref. 68). Bands at  $1663 \pm 4 \text{ cm}^{-1}$ ,  $1671 \pm 3 \text{ cm}^{-1}$ ,  $1683 \pm 2 \text{ cm}^{-1}$ ,  $1689 \pm 2 \text{ cm}^{-1}$ , and  $1694 \pm 2 \text{ cm}^{-1}$  are the result of turns. Antiparallel  $\beta$ -sheets give rise to absorption bands at 1678 and 1688  $\text{cm}^{-1}$  (69), and an absorption band at  $1645 \pm 4 \text{ cm}^{-1}$  has also been found to be associated with unordered secondary structure. IR absorption bands below 1610  $\text{cm}^{-1}$  are generally not associated with amide I transitions and are more likely to be related to amino acid side-chain vibrations (70). Importantly,  $\beta$ -chains do not give rise to amide band frequencies in the approx 1650–1660  $\text{cm}^{-1}$  spectral region (68). Bands at approx  $1653 \pm 4 \text{ cm}^{-1}$  are associated with  $\alpha$ -helical secondary structures and are distinct from those associated with other types of secondary substructure.

The IR absorption spectra of CD2, at 25°C and 90°C in the amide I' spectral region, are

shown in Fig. 5A and B, respectively (bold dashed lines). The second derivative (inverted, shifted, and multiplied by 300) as well as the deconvolved spectra is also shown in Fig. 5A and B. Raising the temperature results in a pronounced “blue”-shift of the peak of the amide I' absorbance spectrum. The second derivative spectrum in Fig. 5A clearly shows an intense peak near 1628  $\text{cm}^{-1}$ . This peak is considerably diminished in intensity upon heating from 25°C to 90°C. This band corresponds to a  $\beta$ -sheet (63,68,69). In addition, the second-derivative spectrum in Fig. 5A at 25°C does not display a distinct band near 1650  $\text{cm}^{-1}$ , but the second-derivative spectrum in Fig. 5B, at 90°C, does. Bands near 1650  $\text{cm}^{-1}$  are routinely associated with  $\alpha$ -helical structure (63). The second-derivative IR spectral data in the amide I' spectral region then indicate qualitatively the loss of  $\beta$ -sheet as the temperature is raised, with the simultaneous formation of an  $\alpha$ -helical secondary structural component.

To investigate these temperature-induced secondary structural changes quantitatively, we have used standard curve-fitting procedures, in conjunction with “resolution enhancing” deconvolution procedures. Figure 5A and B show the deconvolved spectral profiles at 25°C and 90°C, respectively. The peaks in the deconvolved spectral profiles agree particularly well with the peaks in the second-derivative spectra. The deconvolved spectra were resolved into combined Lorentzian and Gaussian components by means of a curve-fitting algorithm that utilizes a Levenberg–Marquardt iteration procedure. The fitted curves in Fig. 5 are virtually identical to the deconvolved spectra. The curve-fit parameters obtained for the 25°C and 90°C deconvolved data are summarized in Table 1. The “goodness of fit” is quantified by a root mean square (RMS) noise parameter. The smaller the RMS noise parameter, the better the fit, or more accurately, the closer the fitted curve matches the data. This is important because it is not possible to visually inspect and judge how well the fitted curves match the data. Clearly, from Fig. 5, any  $\alpha$ -helical components in the protein associated with a band between approx 1649 and

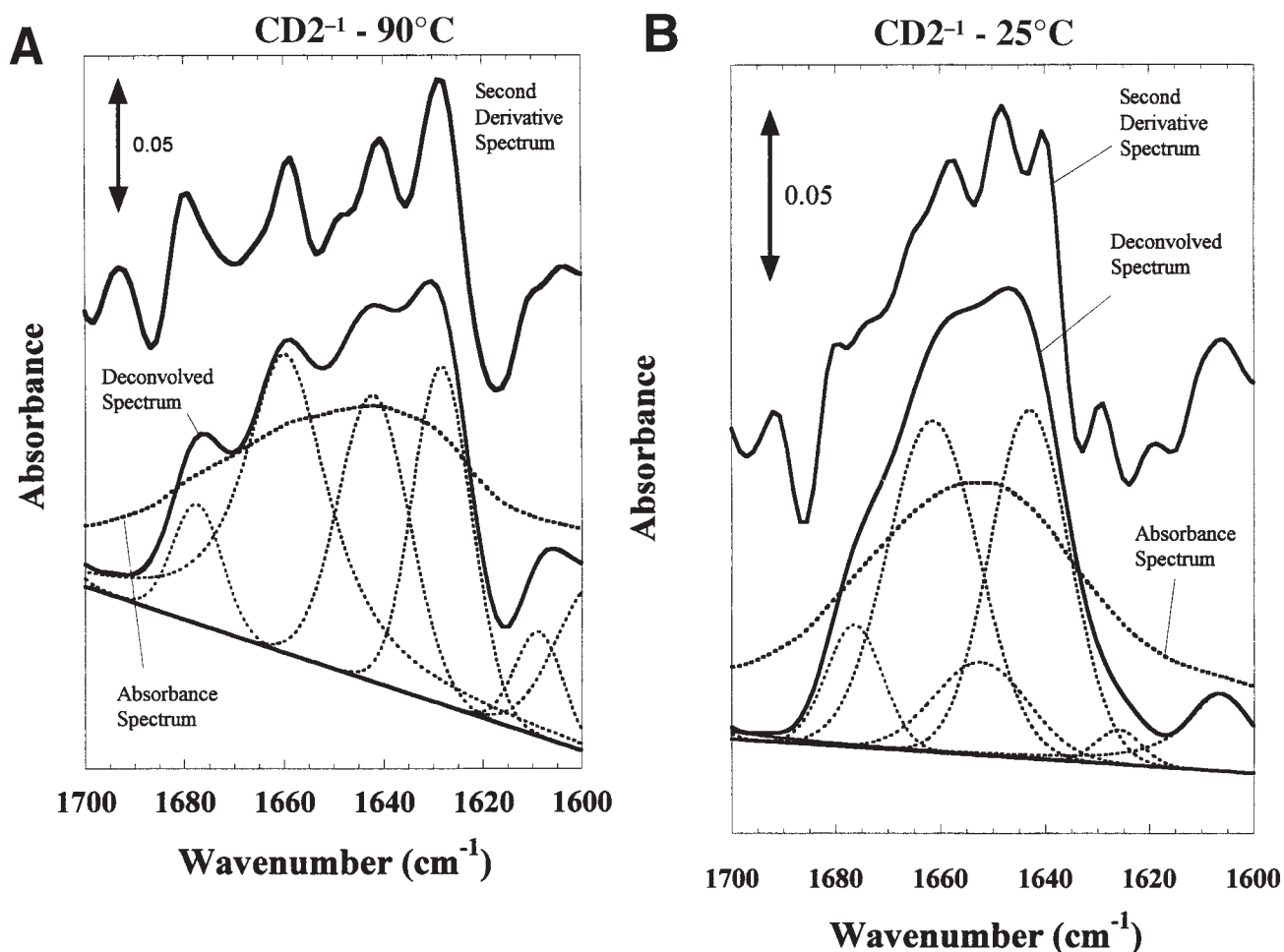


Fig. 5. Infrared absorption spectra (bold dashed lines) of CD2 at (A) 90°C and (B) 25°C in the amide I' spectral region. The second derivative (scaled and shifted) and deconvoluted spectra, obtained from the absorption spectra are also shown. The deconvoluted spectra are fit to a sum of the combined Lorentzian and Gaussian components. The component bands from the fitting are also shown. The fitted curves are indistinguishable from the deconvoluted spectra to the naked eye.

1657  $\text{cm}^{-1}$  could not lead to an accurate description of the 25°C data. This indicates that very little  $\alpha$ -helical substructure is present in CD2-1 at 25°C, in line with far-UV CD data presented here and X-ray structural studies (34–36). Judged by the quantitative RMS noise parameter, we have found that it is *not* possible to find an adequate fit to the 25°C data when a band at 1652  $\text{cm}^{-1}$  is included as either a fixed parameter or a variable starting parameter. If a band at 1652  $\text{cm}^{-1}$  is included as a fixed parameter (with similar intensity and width to the band found at

90°C), the RMS noise is more than a factor of 3 worse than if no such fixed parameter is included (data not shown). Similarly, if a band at 1652  $\text{cm}^{-1}$  is included as a variable starting parameter, the iterative procedure quickly removes the band from this spectral region. On the other hand, a band at 1652  $\text{cm}^{-1}$  (Fig. 5) is required to adequately fit the 90°C data, indicating helix formation at 90°C. The integrated area under each component band and their assignments to secondary structure are also presented in Table 1. Although curve fitting can be some-

Table 1  
Curve-Fit Parameters for CD2-1 Infrared Absorption Spectra at 25°C and 90°C

Position		Integral		Secondary Structure		Assignment
25°C	90°C	25°C	90°C	25°C	90°C	
1596.8		1.300				Amino acid
1608.6	1606.4	0.465	0.544			Amino acid
1615.5	1614.4	0	0			Baseline
1628.1	1626.0	1.815	0.110	24.2%	2.1%	$\beta$ -Sheet
1641.8	1642.8	1.870	1.879	24.9%	36.5%	$\beta$ -Sheet
	<b>1652.0</b>		<b>0.600</b>		<b>11.6%</b>	<b><math>\alpha</math>-Helix</b>
1659.5	1661.3	3.287	2.099	43.8%	40.7%	Turns
1677.3	1676.4	0.536	0.468	7.1%	9.1%	Antiparallel $\beta$ -sheet
1708.7	1709.2	0.200	0.138			
	1724.4		0.545			
		SUM = 7.5	SUM = 5.1			

Note: CD2-1, 25°C, RMS error: 0.000338422. CD2-1, 90°C, RMS error: 0.000344116.

The deconvolved data were fit to eight components plus a baseline. The goodness of fit was characterized using a RMS error parameter. For the 25°C data, the RMS error is  $3.384 \times 10^{-4}$ . For the 90°C data, the RMS error is  $3.44 \times 10^{-4}$ . The term SUM refers to the total integrated area of the bands in the 1625- to 1678-cm<sup>-1</sup> spectral region. Bands outside this region were included in the fit but were not considered in this sum, because they are not related to secondary structure. The percentage secondary structural contribution of each component is estimated by rationing the components integrated area to the total area (or sum). For the present case, the 1652-cm<sup>-1</sup> band contributes approx 11.6% to the total integrated area, which is in a good agreement with 10% helical content from CD studies.

what subjective, there are few possible fits that could accurately describe the FTIR spectra presented here. The signals from helical and random-coil conformations overlap somewhat in FTIR, however, the possibility for a random coil at high temperature is less likely because CD2 has an increased CD signal at 222 nm (structured) instead of the decreased signal at high temperature. The increase of the random coil by high temperature should have resulted in a dramatic decrease in CD signal at 210–250 nm (random coil), which is not what we observed here. The fit presented here is the only possible fit that is compatible with the CD data. The ratio of the band integral to the total integrated area can be used as a measure of the percentage that the secondary structural component contributes to the amide I' absorption band (63,67). The 1652 cm<sup>-1</sup> band of CD2-1 at 90°C is approx 11.6% of the total integrated area in Fig. 5B. This indicates

that in CD2-1, at 90°C, an  $\alpha$ -helical substructure is likely to be formed and it accounts for 11.6% of the secondary substructure of the protein. With the assignments listed in Table 1, it is clear that virtually all of this  $\alpha$ -helical contribution results from loss of  $\beta$ -structures that are associated with the band at 1626–1628 cm<sup>-1</sup>. Taken together, the results from both far-UV CD and FTIR spectral studies indicate the formation of a non-native conformation at high temperatures. It may contain a small population of helical content that appears to be derived from the native  $\beta$ -sheet structure of CD2-1 (H state).

The folding reversibility of this high temperature-induced partially folded state (H state) of CD2-1 was also examined using far and near UV CD and FTIR spectroscopy, at pH 7.3 in PBS buffer. In all types of spectroscopic measurements with different protein concentrations (45–200  $\mu$ M), the spectra of CD2-1 at 25°C

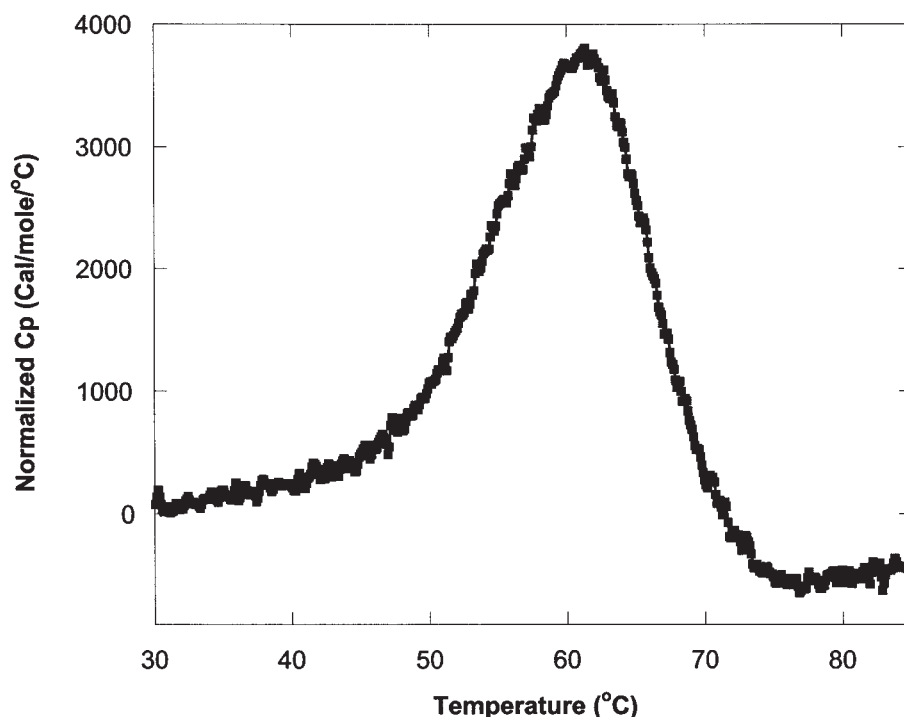


Fig. 6. Microcalorimetry scan for 150  $\mu$ M CD2-1 at pH 7.3 in PBS buffer with a scan rate of 60°C/h.

after heating to 90°C for 30 min is identical to those obtained without heating (Figs. 2A,B, 4). Therefore, the original  $\beta$ -sheet conformation and tight packing of the asymmetric environment of the aromatic amino acid residues of the native state can be regenerated from the partially folded H state. This reversibility upon thermal denaturation allows us to analyze the thermal dynamic properties of CD2-1.

To further investigate the process of thermal denaturation, DSC was applied to monitor the heat-capacity change of CD2-1 during the thermal unfolding process. CD2 exhibits pretransition and posttransition baseline change. Figure 6 shows that there is one peak with a maximum at 62°C from 20°C to 90°C in the heat-capacity transition curve of 150  $\mu$ M CD2-1 at pH 7.3 in PBS buffer with a scan rate of 60°C/h (Fig. 6). The obtained  $T_m$  is consistent with our CD and fluorescence results. We have monitored temperature-induced signal changes at two wavelengths from three structural probes (220 and 230 nm for far-UV CD, 281 and 289 nm for near-UV CD, and

320 and 348 nm for the emission of Trp fluorescence). All unfolding curves have a single transition with a  $T_m$  of about  $61 \pm 1^\circ\text{C}$  (25,51,52,71–73). A simulated curve using the van't Hoff equation based on a two-state transition fits this DSC curve well. The  $\Delta H_{\text{cal}}$  estimated directly from the DSC curve is 50 kcal/mol, which is close to the van't Hoff enthalpy ( $\Delta H_{\text{vH}}$ ) (51 kcal/mol).

#### ***A Random-Coil State of CD2-1 by Chemical Denaturation***

We have also examined the folding and unfolding of CD2-1 by using the chemical denaturant GuHCl. Far-UV CD (180–260 nm), near-UV CD (260–350 nm), and Trp fluorescence spectroscopy have been used to monitor the folding and unfolding processes in CD2-1. Figure 2A shows that the near-UV CD signals at 281 and 291 nm are completely diminished in 6 M GuHCl. Figure 2B shows that the intensity of Trp fluorescence of CD2-1 is dramatically reduced in 6 M GuHCl. Excited at 280 nm, the

emission maxima of CD2-1 is shifted from 318 and 328 to 355 nm. The later wavelength is very similar to that of free amino acid Trp fluorescence (Fig. 2B) and resembles that of completely unfolded proteins (22). Both near-UV CD and Trp fluorescence studies suggest that the tertiary structure of CD2-1 is largely disrupted in 6 M GuHCl. In addition, no enhancement of ANS fluorescence was observed upon the addition of CD2-1 in 6 M GuHCl (data not shown), suggesting that CD2-1 in 6 M GuHCl does not possess exposed hydrophobic clusters (74). As shown in Fig. 4, the far-UV CD spectrum of CD2-1 in 6 M GuHCl closely resembles that of a random-coil conformation (22,27,59), indicating that the secondary structure of CD2-1 is completely unfolded in 6 M GuHCl. Upon removal of GuHCl by dialysis, the far-UV and near-UV CD spectra of the refolded CD2-1 are recovered and are identical to that of the protein without experiencing denaturation (data not shown). The folding and unfolding of CD2-1 by GuHCl is therefore fully reversible. The changes of fluorescence signal at 320 nm, near-UV CD signal at 281 nm, and far-UV CD signal at 220 nm of CD2-1 as a function of GuHCl concentration have a single transition with a  $C_m$  value (50% native at this concentration of GuHCl) of about 2.2 M and can be fitted by a two-state model (data not shown) (51,52,71). Fitting the CD signal change at 230 nm or 289 nm, or the emission of Trp intrinsic fluorescence at 348 nm, as a function of GuHCl concentration (data not shown), all gave similar results. Hence, the conversion of the native state (N state) to the random-coil-like GuHCl denatured state (D state) of CD2-1 by the chemical denaturant GuHCl is highly cooperative in that the change of secondary structure is coupled with that of the tertiary structure and no stable intermediate states are populated. Our results on GuHCl denaturation of CD2-1 agree with the previous studies by Parker et al. (30–33). By monitoring changes in the Trp fluorescence, they reported that the fully folded (N) and unfolded (D) states are the only species populated at equilibrium by GuHCl denaturation. A transient intermediate was suggested to form in

the dead time of the stopped-flow experiment and is unstable.

In summary, all data obtained using different methods suggest that the chemical denatured D state is virtually completely random-coil-like, whereas elevating the temperature induces a partially folded H state of CD2-1. This H state of CD2-1 has largely perturbed tertiary structure and exposed Trp and hydrophobic clusters, which partly resembles the molten-globule state as observed for  $\alpha$ -lactalbumin and myoglobin (8,11,13). On the other hand, we have demonstrated that this H state differs from the classical MG state because it contains a non-native helical conformation with the increase of molar ellipticity at 222 nm and the blue-shifted amide I' IR absorbance band at high temperature, and the conversion from native  $\beta$ -sheet state to an induced H-state of CD2-1 is highly reversible. Similarly, CD2-1 was shown to be significantly helical (43%) in the presence of 80% organic solvent 2,2,2-trifluoroethanol (TFE) (40). Chaotropic agents such as GuHCl and urea bind to the protein and induce an extended unfolded state (75,76). However, high temperatures break H bonds while favoring hydrophobic interactions (49). In the presence of TFE, hydrophobic interactions are altered while intramolecular hydrogen-bonding is promoted (27). Different denaturing factors may have highly diverse effects that do not necessarily populate the same intermediate species (75). The generation of different conformations of CD2-1 under different denaturing conditions results from both the different denaturing factors involved and the non-covalent forces that stabilize CD2-1 (2,75).

### Origin of Conformational Change

To understand the origin of the helical conformation at high temperature, three different computer programs, SOPMA (77), GOR (78), and PHD (79), were used to predict the propensity of secondary structure from the amino acid sequence of CD2-1 (Fig. 1) (40). The native state of CD2-1 has nine  $\beta$ -sheets designated A, B, C, C', C'', D, E, F, and G.  $\beta$ -Strands C' C'' CFG and

DEBA form a two-layer  $\beta$ -sandwich with a conserved core structure (BCEF) (46,80). Residues from four strands, A, B, E, and F, were predicted to have a strong  $\beta$ -sheet preference. In contrast, residues from four strands, GCC' C'', have a strong  $\alpha$ -helix propensity, which is consistent with our observation of the non-native helical conformation at the H state of CD2-1. We propose that these residues with strong helical preferences may be converted to helical conformation by high temperature. At high temperature, the tertiary packing of the protein is largely disrupted, which likely liberates residues on C', C'', and G strands with strong helical preferences to exhibit helical conformations. Further detailed structural analysis by NMR spectroscopy was precluded because CD2-1 was unfortunately found to have a relative low solubility at high temperature (<220  $\mu$ M).

The conformational change between helix and  $\beta$ -sheet in the absence of long-range interactions has also been observed for some other proteins and fragments (57,81–87). A predominant  $\beta$ -sheet protein,  $\beta$ -lactoglobulin, has a markedly high intrinsic preference for an  $\alpha$ -helical structure. An  $\alpha$ -helical intermediate was observed on its way to the formation of the native  $\beta$ -sheet conformation (85). Tumor necrosis factor- $\alpha$  (TNF- $\alpha$ ) is a trimer in which the individual subunits consist of antiparallel  $\beta$ -sheets. Thermal denaturation or the decrease of pH up to 3–4 of TNF- $\alpha$  induces a non-native  $\alpha$ -helical structure (83,88). Similarly, Equinatoxin II, a  $\beta$ -rich protein is converted to a molten-globule state with a well-pronounced  $\alpha$ -rich secondary structure and a complete absence of tertiary structure at low pH values or at high temperature (86). Zhong and Johnson have shown that several sequences with strong  $\alpha$ -helical preference are found to have  $\beta$ -sheet conformation in intact proteins and demonstrated that the secondary conformations of these peptides are strongly dependent on the environment (57).

### ***Implication for Domain Swapping***

Although our equilibrium studies on the unfolding/folding of CD2 do not provide direct

information for the kinetic folding pathway, they do have implications for the key factors contributing to the formation of native structure of  $\beta$ -sheet proteins and provide important information for the conformational flexibility of cell adhesion molecules (32,37). As shown in Fig. 1, these residues on C', C'', and G strands with a helical preference in CD2-1 are highly clustered (such as amino acids from 29 to 49) and located at the hinge region of the two domain-swapping dimers (Fig. 1). Residues with strong  $\beta$ -sheet tendency might initiate the formation of a loosely folded intermediate. On the other hand, residues with helical preferences are likely to be involved in the later stage of the folding of the native  $\beta$ -sheet conformation, which is conducted by long-range interactions relating to the packing of tertiary structure. The slow folding of native  $\beta$ -sheet conformation of these residues with helical preference might allow the loosely folded state of CD2-1 to serve as a template for the formation of a metastable structure of dimeric CD2-1 observed in the GST fusion protein (37). The intermolecular contacts between the loosely folded intermediates can be facilitated in the presence of a dimeric GST fusion partner. This metastable form of CD2-1 illustrates the delicate balance achieved between the formation of single domains or oligomers in both the folding and evolution of IgSF domains (37,39,46,89,90).

## **MATERIALS AND METHODS**

### ***Protein Expression and Purification***

Recombinant rat CD2-1 (residues 1–99) was expressed in LB medium as a fusion construct with the enzyme (GST) of *Schistosoma japonicum* in a pGEX plasmid vector transformed into *Escherichia coli* MC106 (30,34). CD2-1 was first purified as a GST fusion protein using glutathione Sepharose 4B beads (Pharmacia). After being cleaved by thrombin, CD2-1 was further purified using a Superdex 75 column (Pharmacia) in PBS buffer. All of the resultant CD2-1 is monomeric, as assessed by native polyacrylamide gel electrophoresis (PAGE). The

identity of CD2-1 was confirmed by matrix-assisted laser desorption ionization-time of flight (MALDI-TOF) mass spectrometry and amino acid analysis at the core facility of the Centers for Disease Control and Prevention (CDC). The concentration of CD2-1 was measured by its absorption at 280 nm with the extinction coefficient  $\epsilon_{280} = 11,700 \text{ M}^{-1} \text{ cm}^{-1}$  and verified by amino acid analysis at the CDC.

### **CD Spectroscopy**

The CD spectra were measured using a Jasco J710 spectropolarimeter equipped with a temperature-controlled water bath (Neslab 110). CD cells with 1-mm and 10-mm light paths were used for both far- and near-UV CD spectra, respectively. All spectra were the average of eight scans with a scan rate of 50 nm/min. The protein concentration was 45  $\mu\text{M}$  for both the far- and near-UV CD measurements.

### **Trp Fluorescence Spectroscopy**

Fluorescence experiments were performed using a PTI life time fluorimeter equipped with a temperature-controlled water bath (Neslab 110). A fluorescence cell with a 1 cm path length was used. The concentrations used for fluorescence were 2 and 4  $\mu\text{M}$  for CD2-1 and free Trp amino acids, respectively. The scan wavelength for emission spectrum was from 300 to 400 nm with the excitation wavelength at 280 nm. For thermal denaturation, the temperatures in the CD and fluorescence cells were calibrated using a temperature probe (VWR) inserted into the reference cell containing PBS buffer, pH 7.3.

### **ANS Binding Studies**

1-Anilino-naphthalene-8-Sulfonate binding studies were carried out using the same instrument as for Trp fluorescence. The excitation wavelength was 355 nm and fluorescence emission was recorded from 400 to 600 nm with slit width of 2 nm both for excitation and emission. Typically, three scans per spectrum were recorded. ANS stock solution was prepared in water, and the ANS concentration was determined using the molar extinction coefficient

$\epsilon_{350} = 5000 \text{ M}^{-1} \text{ cm}^{-1}$ . Protein and ANS concentrations were varied between 5 and 20 and between 20 and 100  $\mu\text{M}$ , respectively (74).

### **FTIR Spectroscopy**

Static FTIR spectra were recorded using a Bruker IFS66/S spectrometer. The sample was injected between a pair of rectangular  $\text{CaF}_2$  windows ( $38 \times 19 \times 3 \text{ mm}$ ) separated using a dual-compartment (sample and reference) Teflon spacer of 50  $\mu\text{m}$  thickness. A home-built copper cell connected to a water bath that is accurate to 0.1°C was used for temperature-controlled measurements between 12°C and 90°C. For all FTIR measurements, the protein concentration was approx 100  $\mu\text{M}$  in  $\text{D}_2\text{O}$  phosphate buffer. A  $\text{D}_2\text{O}$  reference spectrum was collected at identical temperature, path length, and purge conditions as the protein solution spectrum. This  $\text{D}_2\text{O}$  reference spectrum was subtracted from the protein spectrum at each temperature. This method is essential because  $\text{D}_2\text{O}$  contains temperature-dependent absorption bands in the spectral region of interest (amide I). The static FTIR spectra shown in this work are the average of 10 measurements, each of which consisted of the coaddition of 64 interferograms. No bands related to residual water vapor were observed in the spectra collected between 1700 and 1800  $\text{cm}^{-1}$ . All spectral analysis (subtractions, second derivative calculations, Fourier deconvolution, and curve fitting) was performed using the software package OPUS, supplied by Bruker Instruments.

### **ACKNOWLEDGMENTS**

We would thank Simon Davis, Neil Barclay, and Anthony Clarke for the clones of CD2-1. We thank Mattias Buck, Alec Hodel, Amy Carroll, Robert Cherniak, Mark Dawson, Dabney Dixon, Michael Gross, Zhi-ren Liu, Christina Nugyen, Loren Williams, David Wilson, Wei Yang, Anna Wilkins, and Leanne Isley for critical reading of and comments on the manuscript and helpful discussions. We thank David Hamilton and

Doyle Barrow Jr. for their help on the DSC. We would like to thank Charles Hopper for excellent technical assistance in the construction of accessory components for FTIR temperature studies.

This work was supported in part by GSU start-up funds, quality improvement funds, mentoring grants, and research initiation grants and in part by the NSF grant MCB-0092486 and NIH grant GM62999-1 to JJY and by start-up funds, quality improvement funds, team grants, and research initiation grants to GH from Georgia State University.

## REFERENCES

- Levinthal, C. (1968) Are there pathways for protein folding? *J. Chim. Phys.* **65**, 44–45.
- Dill, K. A. and Chan, H. S. (1997) From Levinthal to pathways to funnels. *Nat. Struct. Biol.* **4**, 10–19.
- Lazaridis, T. and Karplus, M. (1997) *Science* **278**, 1928–1931.
- Kuwajima, K. (1989) The molten globule state as a clue for understanding the folding and cooperativity of globular-protein structure. *Proteins* **6**, 87–103.
- Creighton, T. E. (1991) Characterizing intermediates in protein folding. *Curr. Biol.* **1**, 8–10.
- Radford, S. E., Dobson, C. M., and Evans, P. A. (1992) The folding of hen lysozyme involves partially structured intermediates and multiple pathways. *Nature* **358**, 302–307.
- Fersht, A. (1995) *Phil. Trans. R. Soc. London B: Biol. Sci.* **348**, 11–15.
- Ptitsyn, O. B. (1995) How the molten globule became. *Trends Biochem. Sci.* **20**, 376–379.
- Shortle, D. (1995) Protein Fold recognition. *Nat. Struct. Biol.* **2**, 91–93.
- Dolgikh, D. A., Gilmanshin, R. I., Brazhnikov, E. V., Bychkova, V. E., Semisotnov, G. V., Venyaminov, S. Y., et al. (1981) Alpha-Lactalbumin: compact state with fluctuating tertiary structure? *FEBS Lett.* **136**, 311–315.
- Baum, J., Dobson, C. M., Evans, P. A., and Hanley, C. (1989) Characterization of a partly folded protein by NMR methods: studies on the molten globule state of guinea pig alpha-lactalbumin. *Biochemistry* **28**, 7–13.
- Chyan, C.-L., Wormald, C., Dobson, C. M., Evans, P. A., and Baum, J. (1993) Structure and stability of the molten globule state of guinea-pig alpha-lactalbumin: a hydrogen exchange study. *Biochemistry* **32**, 5681–5691.
- Jennings, P. A. and Wright, P. E. (1993) Formation of a molten globule intermediate early in the kinetic folding pathway of apomyoglobin. *Science* **262**, 892–895.
- Eliezer, D., Yao, J., Dyson, H. J., and Wright, P. E. (1998) *Nat. Struct. Biol.* **5**, 148–155.
- Ohgushi, M. and Wada, A. (1983) 'Molten globule state': a compact form of globular proteins with mobile side-chains. *FEBS Lett.* **164**, 21–24.
- Balbach, J., Forge, V., van Nuland, N. A., Winder, S. L., Hore, P. J., and Dobson, C. M. (1995) Following protein folding in real time using NMR spectroscopy. *Nat. Struct. Biol.* **2**, 865–870.
- Nishii, I., Kataoka, M., and Goto, Y. (1995) Thermodynamic stability of the molten globule states of apomyoglobin. *J. Mol. Biol.* **250**, 223–238.
- Privalov, P. L. (1996) Intermediate states in protein folding. *J. Mol. Biol.* **258**, 707–725.
- Jackson, S. E. and Fersht, A. R. (1991) Folding of chymotrypsin inhibitor 2. 1. Evidence for a two-state transition. *Biochemistry* **30**, 10,428–10,435.
- Viguera, A. R., Martínez, J. C., Filimonov, V. V., Mateo, P. L., and Serrano, L. (1994) Thermodynamic and kinetic analysis of the SH3 domain of spectrin shows a two-state folding transition. *Biochemistry* **33**, 2142–2150.
- Cox, J. P. L., Evans, P. A., Packman, L. C., Williams, D. H., and Woolfson, D. N. (1993) Dissecting the structure of a partially folded protein. Circular dichroism and nuclear magnetic resonance studies of peptides from ubiquitin. *J. Mol. Biol.* **234**, 483–492.
- Khorasanizadeh, S., Peters, I. D., Butt, T. R., and Roder, H. (1993) Folding and stability of a tryptophan-containing mutant of ubiquitin. *Biochemistry* **32**, 7054–7063.
- Clark, P. L., Liu, Z. P., Rizo, J., and Gierasch, L. M. (1997) Cavity formation before stable hydrogen bonding in the folding of a beta-clam protein. *Nat. Struct. Biol.* **4**, 883–886.
- Minor, D. L., Jr. and Kim, P. S. (1994) Context is a major determinant of beta-sheet propensity. *Nature* **367**, 660–663.
- Regan, L. (1994) Protein structure. Born to be beta. *Curr. Biol.* **7**, 656–658.
- Carlsson, U. and Jonsson, B. H. (1995) Folding of beta-sheet proteins. *Curr. Opin. Struct. Biol.* **5**, 482–487.
- Yang, J. J., Buck, M., Pitkeathly, M., Kotik, M., Haynie, D. T., Dobson, C. M., et al. (1995)

- Conformational properties of four peptides spanning the sequence of hen lysozyme. *J. Mol. Biol.* **252**, 483–491.
28. Capaldi, A. P. and Radford, S. E. (1998) Kinetic studies of beta-sheet protein folding. *Curr. Opin. Struct. Biol.* **8**, 86–92.
  29. Mayo, K. H. and Ilyina, E. (1998) A folding pathway for betapep-4 peptide 33 mer: from unfolded monomers and beta-sheet sandwich dimers to well-structured tetramers. *Protein Sci.* **7**, 358–368.
  30. Parker, M. J. and Clarke, A. R. (1997) Amide backbone and water-related H/D isotope effects on the dynamics of a protein folding reaction. *Biochemistry* **36**, 5786–5794.
  31. Parker, M. J., Dempsey, C. E., Lorch, M., and Clarke, A. R. (1997) Acquisition of native beta-strand topology during the rapid collapse phase of protein folding. *Biochemistry* **36**, 13,396–13,405.
  32. Parker, M. J., Dempsey, C. E., Hosszu, L. L., Waltho, J. P., and Clarke, A. R. (1998) Topology, sequence evolution and folding dynamics of an immunoglobulin domain. *Nat. Struct. Biol.* **5**, 194–198.
  33. Parker, M. J., Lorch, M., Sessions, R. B., and Clarke, A. R. (1998) Thermodynamic properties of transient intermediates and transition states in the folding of two contrasting protein structures. *Biochemistry* **37**, 2538–2545.
  34. Driscoll, P. C., Cyster, J. G., Campbell, I. D., and Williams, A. F. (1991) Structure of domain 1 of rat T lymphocyte CD2 antigen. *Nature* **353**, 762–765.
  35. Jones, E. Y., Davis, S. J., Williams, A. F., Harlos, K., and Stuart, D. I. (1992) Crystal structure at 2.8 Å resolution of a soluble form of the cell adhesion molecule CD2. *Nature* **360**, 232–239.
  36. Wyss, D. F., Choi, J. S., Li, J., Knoppers, M. H., Willis, K. J., Arulanandam, A. R., et al. (1995) Conformation and function of the N-linked glycan in the adhesion domain of human CD2. *Science*, **269**, 1273–1278.
  37. Murray, A. J., Lewis, S. J., Barclay, A. N., and Brady, R. L. (1995) One sequence, two folds: a metastable structure of CD2. *Proc. Natl. Acad. Sci. USA* **92**, 7337–7341.
  38. Murray, A. J., Head, J. G., Barker, J. J., and Brady, R. L. (1998) Engineering an intertwined form of CD2 for stability and assembly. *Nat. Struct. Biol.* **5**, 778–782.
  39. Dobson, C. M. (1995) Finding the right fold. *Struct. Biol.* **2**, 513–517.
  40. Yang, J. J., Carroll, A. R., Yang, W., Ye, Y., and Nguyen, C. N. (2000) Nonnative intermediate state of acid-stable beta-sheet protein. *Cell. Biochem. Biophys.* **33**, 253–273.
  41. Woody, R. W. (1985) Circular dichroism of peptides. *Peptides* **7**, 15–114.
  42. Withka, J. M., Wyss, D. F., Wagner, G., Arulanandam, A. R., Reinherz, E. L., and Recny, M. A. (1993) Structure of the glycosylated adhesion domain of human T lymphocyte glycoprotein CD2. *Structure* **1**, 69–81.
  43. Mulkerrin, M. G. (1996) Protein structure analysis using circular dichroism. In *Spectroscopic Method for Determining Protein Structure in Solution*. (Havel, H. A., ed.) New York, VCH.
  44. Capaldi, A. P., Ferguson, S. J., and Radford, S. E. (1999) The Greek key protein apo-pseudoazurin folds through an obligate on-pathway intermediate. *J. Mol. Biol.* **286**, 1621–1632.
  45. Adman, E. T. (1991) Copper protein structures. *Adv. Protein Chem.* **42**, 145–197.
  46. Chothia, C., Gelfand, I., and Kister, A. (1998) Structural determinants in the sequences of immunoglobulin variable domain. *J. Mol. Biol.* **278**, 457–479.
  47. Perczel, A., Park, K., and Fasman, G. D. (1992) Deconvolution of the circular dichroism spectra of protein: the circular dichroism spectra of the antiparallel  $\beta$ -sheet in proteins. *Proteins* **13**, 57–69.
  48. Vuilleumier, S., Sancho, J., Loewenthal, R., and Fersht, A. R. (1993) Circular dichroism studies of barnase and its mutants: characterization of the contribution of aromatic side chains. *Biochemistry* **32**, 10,303–10,313.
  49. Privalov, P. L. and Khechinashvili, N. N. (1974) A thermodynamic approach to the problem of stabilization of globular protein structure: a calorimetric study. *J. Mol. Biol.* **86**, 665–684.
  50. Hagihara, Y., Oobayake, M., and Goto, Y. (1994) Thermal unfolding of tetrameric melittin: Comparison with the molten globule state of cytochrome c. *Protein Sci.* **3**, 1418–1429.
  51. Oliveberg, M., Vuilleumier, S., and Fersht, A. R. (1994) Thermodynamic study of the acid denaturation of barnase and its dependence on ionic strength: evidence for residual electrostatic interactions in the acid/thermally denatured state. *Biochemistry* **33**, 8826–8832.
  52. Gursky, O. and Atkinson, D. (1996) Thermal unfolding of human high-density apolipoprotein A-1: implications for a lipid-free molten globular state. *Proc. Natl. Acad. Sci. USA* **93**, 2991–2995.
  53. Nolting, B., Golbik, R., Soler-Gonzalez, A. S., and Fersht, A. R. (1997) Circular dichroism of dena-

- tured barstar suggests residual structure. *Biochemistry* **36**, 9899–9905.
54. Woody, R. W. (1994) Contributions of tryptophan side chains to the far-ultraviolet circular dichroism of proteins. *Eur. Biophys. J.* **23**, 253–262.
  55. Kurapkat, G., Kruger, P., Wollmer, A., Fleischhauer, J., Kramer, B., Zobel, E., et al. (1997) Calculations of the CD spectrum of bovine pancreatic ribonuclease. *Biopolymers* **41**, 267–287.
  56. Sreerama, N., Manning, M. C., Powers, M. E., Zhang, J. X., Goldenberg, D. P., and Woody, R. W. (1999) Tyrosine, phenylalanine, and disulfide contributions to the circular dichroism of proteins: circular dichroism spectra of wild-type and mutant bovine pancreatic trypsin inhibitor. *Biochemistry* **38**, 10,814–10,822.
  57. Zhong, L. and Johnson, W. C., Jr. (1992) Environment affects amino acid preference for secondary structure. *Pro. Nat. Acad. Sci. USA* **89**, 4462–4465.
  58. Chakrabartty, A., Kortemme, T., Padmanabhan, S., and Baldwin, R. L. (1993) Aromatic side-chain contribution to far-ultraviolet circular dichroism of helical peptides and its effect on measurement of helix propensities. *Biochemistry* **32**, 5560–5565.
  59. Yang, J. J., Pikeathly, M., and Radford, S. E. (1994) Far-UV circular dichroism reveals a conformational switch in a peptide fragment from the beta-sheet of hen lysozyme. *Biochemistry* **33**, 7345–7353.
  60. Susi, H. and Byler, D. M. (1986) Resolution-enhanced fourier transform infrared spectroscopy of enzymes. *Methods Enzymol.* **130**, 290–311.
  61. Haris, P. I. and Chapman, D. (1988) Fourier transform infrared spectra of the polypeptide alamethicin and a possible structural similarity with bacteriorhodopsin. *Biochim. Biophys. Acta.* **943**, 375–380.
  62. Jackson, M., Haris, P. I., and Chapman, D. (1989) Fourier transform infrared spectroscopic studies of lipids, polypeptides and proteins. *J. Mol. Struct.* **214**, 329–355.
  63. Surewicz, W. K., Mantsch, H. H., and Chapman, D. (1993) Determination of protein secondary structure by fourier transform infrared spectroscopy: a critical assessment. *Biochemistry* **32**, 389–394.
  64. Chapman, E. R., An, S., Edwardson, J. M., and Jahn, R. (1996) A novel function for the second C2 domain of synaptotagmin. *J. Biol. Chem.* **271**, 5844–5849.
  65. Zhong, H., Gilmanishin, R., and Callender, R. (1999) An FTIR study of the complex melting behaviour of alpha-lactalbumin. *J. Phys. Chem* **103**, 39,947–39,953.
  66. Troullier, A., Reinstadler, D., Dupont, Y., Naumann, D., and Forge, V. (2000) Transient non-native secondary structures during the refolding of alpha-lactalbumin detected by infrared spectroscopy. *Nat. Struct. Biol.* **7**, 78–86.
  67. Byler, D. M. and Susi, H. (1986) Examination of the secondary structure of proteins by deconvolved FTIR spectra. *Biopolymers* **25**, 469–487.
  68. Susi, H. and Byler, D. M. (1987) Fourier transform infrared study of proteins with parallel beta-chains. *Arch. Biochem. Biophys.* **258**, 465–469.
  69. Fabian, H., Schultz, C., Naumann, D., Landt, O., Hahn, U., and Saenger, W. (1993) Secondary structure and temperature-induced unfolding and refolding of ribonuclease T<sub>1</sub> in aqueous solution. A Fourier transform infrared spectroscopic study. *J. Mol. Biol.* **232**, 967–981.
  70. Chirgadze, Y. N., Fedorov, O. V., and Trushina, N. P. (1975) Estimation of amino acid residue side-chain absorption in the infrared spectra of protein solutions in heavy water. *Biopolymers* **14**, 679–694.
  71. Santoro, M. M. and Bolen, D. W. (1988) Unfolding free energy changes determined by the linear extrapolation method. 1. Unfolding of phenylmethanesulfonyl alpha-chymotrypsin using different denaturants. *Biochemistry* **27**, 8063–8068.
  72. Myers, J. K., Pace, C. N., and Scholtz, J. M. (1995) Denaturant *m* values and heat capacity changes: relation to changes in accessible surface areas of protein unfolding. *Protein Sci.* **4**, 2138–2148.
  73. Kuhlman, B., Boice, J. A., Fairman, R., and Raleigh, D. P. (1998) Structure and stability of the N-terminal domain of the ribosomal protein L9: evidence for rapid two-state folding. *Biochemistry* **37**, 1025–1032.
  74. Yang, J. J., van den Berg, B., Pitkeathly, M., Smith, L. J., Bolin, K. A., Keiderling, T. A., et al. (1996) Native-like secondary structure in a peptide from the alpha-domain of hen lysozyme. *Fold Des.* **1**, 473–484.
  75. Tanford, C. (1968) Protein denaturation. *Adv. Protein Chem.* **23**, 121–282.
  76. Makhatadze, G. I. and Privalov, P. L. (1996) On the entropy of protein folding. *Protein Sci.* **5**, 507–510.
  77. Geourjon, C. and Deleage, G. (1994) SOPM: a self-optimized method for protein secondary structure prediction. *Protein Eng.* **7**, 157–164.

78. Garnier, J., Gibrat, J. F., and Robson, B. (1996) GOR method for predicting protein secondary structure from amino acid sequence. *Methods Enzymol.* **266**, 540–553.
79. Rost, B. and Sander, C. (1993) Prediction of protein secondary structure at better than 70% accuracy. *J. Mol. Biol.* **232**, 584–599.
80. Bork, P., Holm, L., and Sander, C. (1994) The Immunoglobulin fold structural classification, sequence patterns and common core. *J. Mol. Biol.* **242**, 309–320.
81. Hamada, D., Kuroda, Y., Tanaka, T., and Goto, Y. (1995) High helical propensity of the peptide fragments derived from beta- lactoglobulin, a predominantly beta-sheet protein. *J. Mol. Biol.* **254**, 737–746.
82. Shiraki, K., Nishikawa, K., and Goto, Y. (1995) Trifluoroethanol-induced stabilization of  $\alpha$ -helical structure of  $\beta$ -lactoglobulin: implication for non-hierarchical protein folding. *J. Mol. Biol.* **245**, 180–194.
83. Narhi, L. O., Philo, J. S., Li, T., Zhang, M., Samal, B., and Arakawa, T. (1996) Induction of alpha-helix in the beta-sheet protein tumor necrosis factor-alpha: acid-induced denaturation. *Biochemistry* **35**, 11,454–11,460.
84. Narhi, L. O., Philo, J. S., Li, T., Zhang, M., Samal, B., and Arakawa, T. (1996) Induction of alpha-helix in the beta-sheet protein tumor necrosis factor-alpha: thermal- and trifluoroethanol-induced denaturation at neutral pH. *Biochemistry* **35**, 11,447–11,453.
85. Hamada, D., Segawa, S., and Goto, Y. (1996) Non-native alpha-helical intermediate in the refolding of beta- lactoglobulin, a predominantly beta-sheet protein. *Nat. Struct. Biol.* **3**, 868–873.
86. Poklar, N., Lah, J., Salobir, M., Macek, P., and Vesnaver, G. (1997) pH and temperature-induced molten globule-like denatured states of equinatoxin II: a study by UV-melting, DSC, far- and near-UV CD spectroscopy, and ANS fluorescence. *Biochemistry* **36**, 14,345–14,352.
87. Hamada, D. and Goto, Y. (1997) The equilibrium intermediate of beta-lactoglobulin with non-native alpha-helical structure *J. Mol. Biol.* **269**, 479–487.
88. Narhi, L. O., Rosenfeld, R., Wen, J., Arakawa, T., Prestrelski, S. J., and Philo, J. S. (1993) Acid-induced unfolding of brain-derived neurotrophic factor results in the formation of a monomeric 'A state'. *Biochemistry* **32**, 10,819–10,825.
89. Bennett, M. J., Schlunegger, M. P., and Eisenberg, D. (1995) 3D domain swapping: a mechanism for oligomer assembly. *Protein Sci.* **4**, 2455–2468.
90. Schlunegger, M. P., Bennett, M. J., and Eisenberg, D. (1997) Oligomer formation by 3D domain swapping: a model for protein assembly and misassembly *Adv. Protein Chem.* **50**, 61–122.